Hfs of F^{19} in the Electron Paramagnetic Resonance of $Mn:ZnF_2$

A. M. CLOGSTON, J. P. GORDON, V. JACCARINO, M. PETER, AND L. R. WALKER
Bell Telephone Laboratories, Murray Hill, New Jersey

(Received September 17, 1959)

An experimental and theoretical re-examination of the F^{19} "super-hfs" in the electron paramagnetic resonance (EPR) of Mn^{++} as a dilute, substitutional impurity in ZnF_2 has been made. The observation of anomalous spectra at 23 kMc/sec has necessitated a modification of the phenomenological theory first offered by Tinkham. Precise measurement of all of the hfs interaction constants, in conjunction with the new theory, allows direct comparison to be made with the results of the NMR experiments of F^{19} in MnF_2. The agreement now found is most satisfactory. The theory of the origin of the F^{19} hfs is discussed in the light of recent work of Mukherji and Das, Marshall, and Keffer *et al.*

The Mn^{55} hfs was measured and found to be anisotropic. This, in conjunction with Mn^{55} specific heat measurements in antiferromagnetic MnF_2, enables one to compute the magnetization of a sublattice at $T=0°K$.

INTRODUCTION

TINKHAM[1] has observed the electron paramagnetic resonance (EPR)[2] of Mn^{++} as a dilute, substitutional impurity in the diamagnetic ZnF_2 lattice. The unusual nature of this spectrum stems from the fact that, in addition to the now commonly observed Mn^{55} hfs, there is superimposed on each Mn^{55} hyperfine component an extensive "super-hfs." This latter structure results from the hfs interaction of the nonlocalized magnetic electrons of the central Mn^{++} ion with the nuclei of the octahedra of nominally diamagnetic F^- ions that surround the paramagnetic ion. From these observations an attempt was made[3] to interpret the distribution of magnetic electrons using a molecular-orbital treatment as Owen[4] had done previously in treating charge-transfer in octahedral complexes.

Closely related to this are the observed large shifts in the NMR[5] of F^{19} in the isomorphic MnF_2 lattice. The spatial distribution of magnetic electrons causes, in the antiferromagnetic state, an appearance of the NMR at very high frequencies even in the absence of an external magnetic field.[6,7] It was, indeed, a consideration of the relation of these phenomena that motivated this more detailed re-examination of the EPR spectrum.

ZnF_2 belongs to the rutile class of crystals which exhibit macroscopic tetragonal symmetry. Since the local symmetry of a Zn^{++} site is only orthorhombic, the tetragonal character results from the axes of the two Zn ions in a unit cell being rotated by 90° about the c axis from each other. This feature, which adds more complexity to the EPR spectrum, is depicted in Fig. 1. It is to be noted that if the field lies in the a-c, or (010), plane the two sites become equivalent. Relevant parameters for the ZnF_2 and MnF_2 lattices are given in Table III.[8]

SPIN HAMILTONIAN

The ground state of the Mn^{++} ion is $(3d^5)^6S$ and in a crystalline field of orthorhombic symmetry was described in an approximate fashion by Tinkham by using the spin Hamiltonian

$$\mathcal{H}=g\beta\mathbf{H}\cdot\mathbf{S}+\mathbf{S}\cdot D\cdot\mathbf{S}+A^{55}\mathbf{I}\cdot\mathbf{S}, \qquad (1)$$

assuming g and A^{55} to be isotropic.

In consideration of the length of our more detailed presentation our attentions were confined to a precise measurement of the F^{19} and Mn^{55} hfs. Only the sign of the crystal field parameters was confirmed by observing the variation of the intensities of appropriate transitions at low temperatures. Tinkham's values for the components of the D tensor and the value of g were

$$D_x=(23\pm15)g \quad D_y=(110\pm10)g,$$
$$D_z=-(133\pm5)g \quad g=2.002\pm0.005.$$

The Mn^{55} hyperfine interaction constant was remeasured and found not to agree with Tinkham's result of $A=(103\pm3)g$. This will be discussed more fully later.

EXPERIMENTAL METHODS

The experiments were performed on single crystals of ZnF_2, obtained from Professor J. W. Stout,[9] in two frequency regions; 23 kMc and 54 kMc.

The 23-kMc apparatus employs a high-Q ($\simeq$15 000

[1] M. Tinkham, Proc. Roy. Soc. (London) **A236**, 535 (1956).
[2] The experiments of Tinkham were performed at 9 kMc (private communication to V. Jaccarino).
[3] M. Tinkham, Proc. Roy. Soc. (London) **A236**, 549 (1956).
[4] J. Owen, Discussions Faraday Soc. **19**, 127 (1955). Reference will be found here to earlier work of Griffiths and Owen and the theory of Stevens.
[5] R. G. Shulman and V. Jaccarino, Phys. Rev. **103**, 1126 (1956); **108**, 1219 (1957), B. Bleaney, Phys. Rev. **104**, 1190 (1956).
[6] V. Jaccarino and R. G. Shulman, Phys. Rev. **107**, 1196 (1957); V. Jaccarino and L. R. Walker in *Colloque International de Magnétisme* (Centre National de la Recherche Scientifique, Paris, 1959).
[7] V. Jaccarino and L. R. Walker, (to be published).
[8] The structure parameters of the iron group difluorides are given in J. W. Stout and S. A. Reed, J. Am. Chem. Soc. **5**, 5279 (1954) and more recently by W. H. Baur, Acta Cryst. **11**, 488 (1958).
[9] The principal magnetic impurities were in weight percent (approximately); 0.04 Ni, 0.03 Mn, and 0.03 Fe. The crystals were grown by Reed and Stout with the hope, originally, of observing the Ni^{++} spectrum at millimeter wave frequencies.

unloaded) reflection cavity and superheterodyne detection. The cylindrical cavity, whose axis is vertical, operates in the TE_{011} mode with the sample being supported on a Lucite rod in the central maximum of the rf magnetic field. A 12-inch Varian magnet, rotatable in the horizontal plane, provides the necessary dc magnetic field (H_0). The samples were oriented so that H_0 could be rotated in either the (110) or (001) planes.

A novel feature of this spectrometer is a mechanism (suggested by R. Kompfner) that allows the external coupling of the cavity to be varied during operation and thereby eliminates the need for a microwave bridge.[10] Maximum sensitivity is achieved by operating very near to the matched condition where no power is reflected. Sensitivity to either the real or imaginary parts of the sample susceptibility is achieved by small purposeful departures from critical match. An unbalance achieved by changing the coupling permits observation of the imaginary (absorptive) component, while an unbalance produced by a shift in frequency of the signal klystron permits observation of the real (dispersive) component.

At 77°K the absorption signal was sufficiently intense to allow a relatively noise-free oscilloscope (CRO) presentation of the second detector crystal output using a synchronous magnetic field modulation of up to 25 gauss peak-to-peak. Orientation of the crystal in the plane of the field could be quickly obtained, to an accuracy of better than 0.5° by symmetrizing the CRO display. A Numar NMR gauss meter was used for precise measurements of the dc magnetic field. A dual channel CRO allowed simultaneous display of EPR and NMR signals thereby facilitating the field measurements.

The 54-kMc apparatus is a noncavity transmission type spectrometer[11] employing a backward-wave oscillator as a signal source and single crystal rf detection and audio demodulation. For purposes of adequate sensitivity small field modulation and phase-sensitive detection were employed, with the spectra displayed on a chart recorder. Observations were made at 77°, 14°, and 4°K.

PHENOMENOLOGICAL THEORY OF THE F^{19} hfs

General Considerations

The hfs interaction of the F^{19} nuclei with the nonlocalized spin magnetization of the Mn^{++} ion may be described by adding to the spin Hamiltonian a term of the form

$$\mathcal{H}^{19}=\sum_i \mathbf{S}\cdot A^i\cdot\mathbf{I}_i, \qquad (2)$$

where the summation is to be taken over the six neighboring F^{19} nuclei.

[10] J. P. Gordon (a more complete discussion of the spectrometer will be published elsewhere).
[11] M. Peter, Phys. Rev. **113**, 801 (1959).

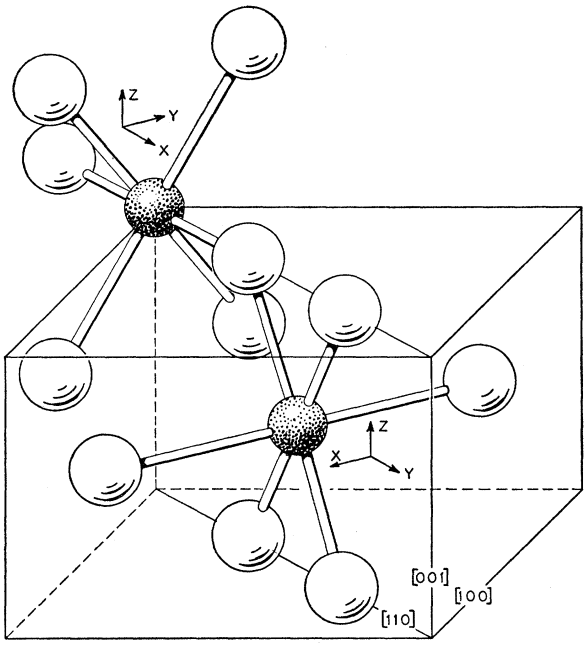

FIG. 1. A diagrammatic representation of the two nonequivalent cation sites in the ZnF_2 lattice. The local system of axes for each Mn^{++} (dark) is given and is seen to differ from site to site only by a 90° rotation of the surrounding F^- (light) octahedron about the [001] direction. The three *crystalline* directions along which the magnetic field was placed are indicated in the lower right-hand corner of the figure. The distortion of each octahedron leaves the anion crystalline field with only orthorhombic symmetry at the Mn^{++} position.

Before pursuing the phenomenological description we digress to consider various interpretations that have been given of the origin of the hfs interaction. In his paper on Mn:ZnF_2, Tinkham ascribed the effect to covalent bonding between the metal ions and fluorine ions. According to this picture, the metal ion *d*-wave functions have augmented to them small amounts of ligand wave functions of the proper symmetry to form antibonding orbitals, while the ligand wave functions are similarly augmented with *d*-wave functions to form bonding orbitals. The bonding orbitals are filled with paired electron spins and give no net contribution to the fluorine hyperfine interaction. The unpaired *d* electrons, however, spread out in the antibonding orbitals and produce the observed interaction. This was also the point of view of Stevens, and of Griffiths and Owen, in discussing the hyperfine structure of the spin resonance of Ir^{4+} ions in the chloroplatinates.

In their first paper on the fluorine nuclear resonance in MnF_2, Shulman and Jaccarino[5] used a different point of view closely related to the superexchange mechanisms discussed by Kramers and Anderson. In this picture, the ground-state configuration has unpaired electrons in the *d* states and paired electrons in the fluorine *p* and *s* states. Excited configurations are then introduced in which an electron is transferred from occupied fluorine states into a *d* state wave

function. The hyperfine interaction is ascribed to the remaining unpaired electrons in fluorine wave functions. This picture is incomplete in that it ignores a contribution to the hyperfine interactions already present in the ground-state configuration due to the nonorthogonality of the metal ion and ligand wave functions.

Recently several attempts have been made to calculate the fluorine hyperfine interaction from first principles. Mukherji and Das,[12] for example, proceed by orthogonalizing the d wave functions to the ligand wave functions. The resultant, distorted d wave function is then used to calculate the interaction, just as in the covalent bonding picture. This gives a result that depends only upon the overlap of the d wave functions and ligand wave functions, and which is just the nonorthogonality effect discussed above. This calculation neglects, however, the electron transfer effect.

A unified treatment of the problem, which includes both contributions to the hyperfine interaction, has been given very recently by Keffer *et al.*[13] They begin with a set of nonorthogonal d and ligand wave functions for the ground state, and then calculate by second-order perturbation theory how much of the various excited transfer configurations must be added. A proper calculation of the fluorine hyperfine interaction then yields both orthogonality and transfer effects.

In order to understand more clearly the basis of the phenomenological treatment of the experimental results of the present experiments, let us consider briefly a very simple two-center problem exhibiting the effects discussed above. Imagine a wave function ψ centered at point 1 occupied by a single electron, and a wave function φ centered at point 2 and occupied by two electrons.

For ease in calculation we introduce a wave function $\theta=(1-S^2)^{-\frac{1}{2}}(\psi-S\varphi)$ where S is the overlap integral between ψ and φ. The wave function of the system including transfer effects is $(\theta^+\varphi^+\varphi^-)+\lambda(\theta^+\theta^-\varphi^+)$, where λ is calculated by second-order perturbation theory, and the plus and minus signs indicate the direction of electron spin. This wave function may be used to calculate the hyperfine interaction with a nucleus situated at point 2. The result is proportional to $(S+\lambda)^2$, where S is the overlap effect and λ the transfer effect. In very simplified form, this is the calculation carried out by Keffer *et al.*

An entirely equivalent point of view is the following. We adopt three wave functions

$$\begin{aligned}\alpha^+&=(1+2aS+a^2)^{-\frac{1}{2}}(\varphi^++a\psi^+),\\ \beta^+&=(1+2bS+b^2)^{-\frac{1}{2}}(b\varphi^++\psi^+),\\ \gamma^-&=(1+2cS+c^2)^{-\frac{1}{2}}(c\varphi^-+\psi^-).\end{aligned}\tag{3}$$

Wave functions α^+ and β^+ are made orthogonal by demanding $(b+a)+(ab+1)S=0$. The wave function γ^- is already orthogonal to the other two by virtue of its spin. We now find the best values of a, b, and c by minimizing the energy. If we imagine a determinantal wave function formed from $\alpha^+\beta^+\gamma^-$, one can readily show that neither the energy or hyperfine interaction can depend upon a or b. Consequently, the minimization problem depends entirely upon c and determines a value $c=\lambda$. The total hyperfine interaction is again $(S+\lambda)^2$, to second order.

We may now relate this approach to the idea of covalent bonding. Since the system is independent of b, we may as well choose $b=c$. Wave functions β^+ and γ^- then become the *filled* bonding orbital and give no net contribution to the hyperfine interaction. The total interaction is therefore proportional to a^2, which by the orthogonality relation is just $(S+\lambda)^2$, as before.

In this paper we shall adopt the covalent bonding point of view in constructing a phenomenological description of the fluorine hyperfine interaction. Consequently, the entire burden of the interaction will rest upon the augmented d wave functions.

We shall first, in the next two sections, express the hyperfine constants in terms of the augmentation parameters of the wave functions, and then in the final section, discuss the spin resonance spectrum that results from the fluorine hyperfine interaction.

AUGMENTED WAVE FUNCTIONS

The geometry with which we shall be concerned is shown in Fig. 2(a) where we may see a manganese ion Mn^{++} surrounded by six fluorine ions F^-, arranged on a distorted octahedron having orthorhombic symmetry. The F^- positions are numbered for purposes of identification.

We note first that the structure given in Fig. 2(a) belongs to the point group D_{2h}. This group has eight one-dimensional representations, four of even parity and four of odd parity. Using the notation of Koster,[14] we denote the four even representations by η_1, η_2, η_3, and η_4. The manganese d wave functions form a representation of the group as follows:

$$\begin{aligned}
d_1&=(15/16\pi)^{\frac{1}{2}}(2x^2-z^2-y^2)(1/r^2)R && \text{belongs to } \eta_1,\\
d_2&=(15/16\pi)^{\frac{1}{2}}(z^2-y^2)(1/r^2)R && \text{belongs to } \eta_1,\\
d_3&=(15/4\pi)^{\frac{1}{2}}xy(1/r^2)R && \text{belongs to } \eta_3,\\
d_4&=(15/4\pi)^{\frac{1}{2}}zx(1/r^2)R && \text{belongs to } \eta_2,\\
d_5&=(15/4\pi)^{\frac{1}{2}}yz(1/r^2)R && \text{belongs to } \eta_4,
\end{aligned}\tag{4}$$

where R is the normalized hydrogenic radial wave function for $n=3$ and $l=2$.

If we consider only $2s$ and $2p$ wave functions of the fluorine ions, we have a total of six $2s$ wave functions

[12] A. Mukherji and T. P. Das, Phys. Rev. **111**, 1479 (1958); W. Marshall, Bull. Am. Phys. Soc. **4**, 142 (1959).

[13] F. Keffer, T. Oguchi, W. O'Sullivan, and J. Yamashita, Phys. Rev. **115**, 1553 (1959).

[14] G. Koster in *Solid State Physics*, edited by F. Seitz and D. Turnbull (Academic Press, Inc., New York, 1957), Vol. 5.

and 18 $2p$ wave functions. The $2s$ wave functions form even representations of the group as below:

$$\begin{aligned}
&(1/\sqrt{2})(s_5+s_6) && \text{belongs to } \eta_1,\\
&\tfrac{1}{2}(s_1+s_2+s_3+s_4) && \text{belongs to } \eta_1,\\
&\tfrac{1}{2}(s_1-s_2+s_3-s_4) && \text{belongs to } \eta_4,
\end{aligned} \tag{5}$$

where the subscripts refer to particular centers as assigned in Fig. 2(a). The normalization of these wave functions assumes explicitly that the overlap integrals are negligible.

The representations formed from p functions are considerably more complicated. We designate the various wave functions according to the scheme given in Figs. 2(b) and 2(c) where the positive lobe carries the label in each case. *Since no symmetry requirements dictate a special choice for the directions of the σ and μ orbitals, we allow them to lie on the z and y axes, respectively.*

$$\begin{aligned}
&(1/\sqrt{2})(\sigma_5+\sigma_6) && \text{belongs to } \eta_1,\\
&\tfrac{1}{2}(\mu_1+\mu_2+\mu_3+\mu_4) && \text{belongs to } \eta_1,\\
&\tfrac{1}{2}(\sigma_1+\sigma_2+\sigma_3+\sigma_4) && \text{belongs to } \eta_1,\\
&(1/\sqrt{2})(\mu_6+\mu_5) && \text{belongs to } \eta_2,\\
&\tfrac{1}{2}(\pi_1+\pi_2-\pi_3-\pi_4) && \text{belongs to } \eta_2,\\
&(1/\sqrt{2})(\pi_6-\pi_5) && \text{belongs to } \eta_3,\\
&\tfrac{1}{2}(\pi_1-\pi_2-\pi_3+\pi_4) && \text{belongs to } \eta_3,\\
&\tfrac{1}{2}(\mu_1-\mu_2+\mu_3-\mu_4) && \text{belongs to } \eta_4,\\
&\tfrac{1}{2}(\sigma_1-\sigma_2+\sigma_3-\sigma_4) && \text{belongs to } \eta_4,
\end{aligned} \tag{6}$$

The augmented d wave functions can now be written down by combining wave functions belonging to the same representation. We obtain

$$\begin{aligned}
D_1=&N_1[d_1+(\alpha_1/\sqrt{2}(s_5+s_6)+\beta_1/2(s_1+s_2+s_3+s_4)\\
&+(\gamma_1/\sqrt{2}(\sigma_5+\sigma_6)+(\delta_1/2)(\mu_1+\mu_2+\mu_3+\mu_4)\\
&+(\epsilon_1/2)(\sigma_1+\sigma_2+\sigma_3+\sigma_4)],\\
D_2=&N_2[d_2+(\beta_2/2)(s_1+s_2+s_3+s_4)\\
&+(\delta_2/2)(\mu_1+\mu_2+\mu_3+\mu_4)\\
&+(\epsilon_2/2)(\sigma_1+\sigma_2+\sigma_3+\sigma_4)],\\
D_3=&N_3[d_3+(\alpha_3/\sqrt{2})(\pi_6-\pi_5)\\
&+(\beta_3/2)(\pi_1-\pi_2-\pi_3+\pi_4)],\\
D_4=&N_4[d_4+(\alpha_4/\sqrt{2})(\mu_6-\mu_5)\\
&+(\beta_4/2)(\pi_1+\pi_2-\pi_3-\pi_4)],\\
D_5=&N_5[d_5+(\alpha_5/2)(s_1-s_2+s_3-s_4)\\
&+(\beta_5/2)(\mu_1-\mu_2+\mu_3-\mu_4)\\
&+(\gamma_5/2)(\sigma_1-\sigma_2+\sigma_3-\sigma_4)].
\end{aligned} \tag{7}$$

It should be noted that D_1 and D_2 are not automatically orthogonal by symmetry. In order to insure this orthogonality, one relation must exist amongst the augmentation parameters of D_1 and D_2.

FLUORINE HYPERFINE INTERACTION

The electron spin-fluorine nucleus interaction Hamiltonian is,[15]

$$\mathcal{H}^{19}=g\beta\gamma\beta_N\sum_{ka}\left(-\frac{\mathbf{S}_k\cdot\mathbf{I}_a}{r_{ka}^3}+\frac{3(\mathbf{r}_{ka}\cdot\mathbf{S}_k)(\mathbf{r}_{ka}\cdot\mathbf{I}_a)}{r_{ka}^5}+\frac{8\pi}{3}\delta(r_{ka})\mathbf{S}_k\cdot\mathbf{I}_a\right), \tag{8}$$

where r_{ka} is the electron-nucleus distance and k is summed over electrons and a over nuclei. We shall be concerned with a manifold of electronic states where one electron occupies each of the states D_1, D_2, D_3, D_4, D_5 with spins aligned to give a total spin $S=\frac{5}{2}$. Within this ground manifold, we may easily show by an application of the Wigner-Eckart theorem that (6) is equivalent to

$$\mathcal{H}^{19}=g\beta\gamma\beta_N\frac{1}{5}\sum_{na}\left(D_n\left|-\frac{\mathbf{S}\cdot\mathbf{I}_a}{r_a^3}+\frac{3(\mathbf{r}_a\cdot\mathbf{S})(\mathbf{r}_a\cdot\mathbf{I}_a)}{r_a^5}+\frac{8\pi}{3}\delta(r_a)\mathbf{S}\cdot\mathbf{I}_a\right|D_n\right), \tag{9}$$

where n sums over wave functions, a over nuclei, and r_a is the electron-nucleus distance.

Let us define the following quantities:

$$U_a=g\beta\gamma\beta_N\frac{1}{5}\left(-\frac{\mathbf{S}\cdot\mathbf{I}_a}{r_a^3}+\frac{3(\mathbf{r}_a\cdot\mathbf{S})(\mathbf{r}_a\cdot\mathbf{I}_a)}{r_a^5}\right), \tag{10}$$

$$V_a=g\beta\gamma\beta_N\tfrac{1}{5}(8\pi/3)\delta(r_a)\mathbf{S}\cdot\mathbf{I}_a, \tag{11}$$

$$\begin{aligned}
&F_s=(N_1\beta_1/2)^2+(N_2\beta_2/2)^2+(N_5\alpha_5/2)^2, && f_s=(N_1\alpha_1)^2/2,\\
&F_\mu=(N_1\delta_1/2)^2+(N_2\delta_2/2)^2+(N_5\beta_5/2)^2, && f_\mu=(N_4\alpha_4)^2/2,\\
&F_\sigma=(N_1\epsilon_1/2)^2+(N_2\epsilon_2/2)^2+(N_5\gamma_5/2)^2, && f_\sigma=(N_1\gamma_1)^2/2,\\
&G_{\mu\sigma}=(N_1\delta_1/2)(N_1\epsilon_1/2)+(N_2\delta_2/2)(N_2\epsilon_2/2)+(N_5\beta_5/2)(N_5\gamma_5/2),\\
&F_\pi=(N_3\beta_3/2)^2+(N_4\beta_4/2)^2, \quad F_\pi=(N_3\alpha_3)^2/2,\\
&F=5-4(F_s+F_\mu+F_\sigma+F_\pi)-2(f_s+f_\mu+f_\sigma+f_\pi).
\end{aligned} \tag{12}$$

The fluorine hyperfine interaction (9) can then be

[15] $\gamma\beta_N\equiv-\gamma^{19}$.

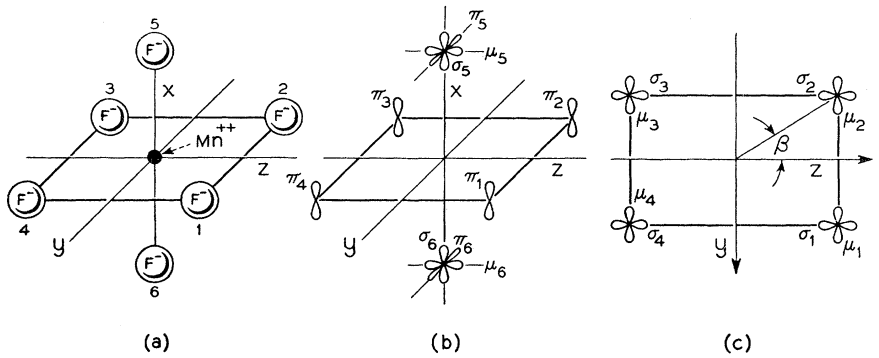

FIG. 2. A diagrammatic representation of the isotropic and anisotropic character of the F^- wave functions. The nomenclature and orientation of the wave functions are explained in the text.

written

$$\mathcal{H}^{19}=g\beta\gamma\beta_N\Big\{\frac{F}{5}\sum_a\Big[-\frac{\mathbf{S}\cdot\mathbf{I}_a}{R_a^3}+\frac{3(\mathbf{R}_a\cdot\mathbf{S})(\mathbf{R}_a\cdot\mathbf{I}_a)}{R_a^5}\Big]$$
$$+\sum_{a=1,2,3,4}[F_s(s_a|V_a|s_a)+F_\mu(\mu_a|U_a|\mu_a)$$
$$+F_\sigma(\sigma_a|U_a|\sigma_a)+F_\pi(\pi_a|U|\pi_a)]$$
$$+2G_{\mu\sigma}(\mu_a|U_a|\sigma_a)+\sum_{a=5,6}[f_s(s_a|V_a|s_a)$$
$$+f_\mu(\mu_a|U_a|\mu_a)+f_\sigma(\sigma_a|U_a|\sigma_a)$$
$$+f_\pi(\pi_a|U_a|\pi_a)]\Big\}. \quad (13)$$

Here R_a is the distance from the manganese ion to fluorine ion a. All electron charge density not represented in fluorine wave functions is considered to be spherically distributed about the manganese center.

We may now proceed from Eq. (13) to write out explicitly the interaction tensor A in the coordinate system chosen in Fig. 1. We designate nuclei 2 and 4 to be of type I, 1 and 3 of type I′, and 5 and 6 of type II, and obtain the components listed in Tables I and II. The interactions for type I′ nuclei are obtained by reversing the sign of β. In Table I we note the presence of the off-diagonal component A_{yz} which was neglected by Tinkham and is important in what follows.

We now introduce some further definitions

Let

$$A_D^{\rm I}=g\beta\gamma\beta_N(F/5)1/R_{\rm I}^3,$$
$$A_s^{\rm I}=g\beta\gamma\beta_N(F_s/5)(8\pi/3)|s(0)|^2,$$
$$A_\sigma^{\rm I}=g\beta\gamma\beta_N(2/25)\langle 1/r^3\rangle|[G_{\mu\sigma}{}^2+(F_\sigma-F_\mu)^2]^{\frac{1}{2}}|,$$
$$A_\pi^{\rm I}=g\beta\gamma\beta_N(2/25)\langle 1/r^3\rangle\tfrac{1}{2}\{|[G_{\mu\sigma}{}^2+(F_\sigma-F_\mu)^2]^{\frac{1}{2}}|$$
$$-F_\mu-F_\sigma+F_\pi\},$$
$$\tan 2\alpha=G_{\mu\sigma}/(F_\sigma-F_\mu), \quad (14)$$
$$A_D^{\rm II}=g\beta\gamma\beta_N(F/5)(1/R_{\rm II}^3),$$
$$A_s^{\rm II}=g\beta\gamma\beta_N(f_s/5)(8\pi/3)|s(0)|^2,$$
$$A_\sigma^{\rm II}=g\beta\gamma\beta_N(2/25)\langle 1/r^3\rangle(f_\sigma-f_\mu),$$
$$A_\pi^{\rm II}=g\beta\gamma\beta_N(2/25)\langle 1/r^3\rangle(f_\pi-f_\mu).$$

It follows then from Eq. (12) and Tables I and II that

$$A_{xx}^{\rm I}=A_s^{\rm I}-A_D^{\rm I}-A_\sigma^{\rm I}+2A_\pi^{\rm I},$$
$$A_{yy}^{\rm I}=A_s^{\rm I}+(3\sin^2\beta-1)A_D^{\rm I}$$
$$+(3\sin^2\alpha-1)A_\sigma^{\rm I}-A_\pi^{\rm I},$$
$$A_{zz}^{\rm I}=A_s^{\rm I}+(3\cos^2\beta-1)A_D^{\rm I} \quad (15)$$
$$+(3\cos^2\alpha-1)A_\sigma^{\rm I}-A_\pi^{\rm I},$$
$$A_{yz}^{\rm I}=-3\sin\beta\cos\beta A_D^{\rm I}-3\sin\alpha\cos\alpha A_\sigma^{\rm I},$$

and

$$A_{xx}^{\rm II}=A_s^{\rm II}+2A_D^{\rm II}+2A_\sigma^{\rm II}-A_\pi^{\rm II},$$
$$A_{yy}^{\rm II}=A_s^{\rm II}-A_D^{\rm II}-A_\sigma^{\rm II}+2A_\pi^{\rm II}, \quad (16)$$
$$A_{zz}^{\rm II}=A_s^{\rm II}-A_D^{\rm II}-A_\sigma^{\rm II}-A_\pi^{\rm II}.$$

The $A^{\rm I}$ tensor is now seen to consist of four parts; one, of strength $A_D^{\rm I}$, is the dipole field of the manganese magnetization and involves the actual bond angle, β; there is an isotropic part of strength $A_s^{\rm I}$; the term proportional to $A_\pi^{\rm I}$ arises from an effective magnetic dipole in the x direction and the remaining contribution is that of an effective magnetic dipole in the yz plane of strength $A_\sigma^{\rm I}$ making an angle α with the z axis. The $A^{\rm II}$ tensor may be resolved in a similar way.

PREDICTED SPECTRA

That part of the complete spin Hamiltonian of the system which depends upon the F^{19} nuclei will be the sum of six terms, one for each independent F^{19} nucleus. Each of these may be written in the form

$$H_i=\mathbf{I}_i\cdot A^i\cdot\mathbf{S}+\gamma\beta_N H_0(\mathbf{I}_i\cdot\mathbf{n}) \quad (17)$$

$i=1, 2, \cdots, 6$, where A^i is the hyperfine tensor appropriate to the ith nucleus and $H_0\mathbf{n}$ is an applied field of magnitude H_0. For sufficiently large H_0 we may replace $A_i\cdot\mathbf{S}$ by $mA^i\cdot\mathbf{n}$, where m is the projection quantum number of $\mathbf{S}$ along $\mathbf{n}$. The individual nuclei are now quantized along an effective magnetic field, $H_0\mathbf{n}+(m/\gamma\beta_N)A^i\cdot\mathbf{n}$. Unless $A_i\cdot\mathbf{n}$ happens to be parallel to $\mathbf{n}$, the direction of this field will depend upon m, shifting when an electronic transition occurs. Either nuclear state for a given m will have a projection upon each of the nuclear states for any other m value. It follows that in a $(m\leftrightarrow m+1)$ electronic transition,

TABLE I. Type I.

A_{xx}	A_{yy}	A_{zz}	A_{yz}	Times
-1	$3\sin^2\beta-1$	$3\cos^2\beta-1$	$-3\sin\beta\cos\beta$	$g\beta\gamma\beta_N(F/5)(1/R_{\rm I}^3)$
1	1	1	0	$g\beta\gamma\beta_N(F_s/5)(8\pi/3)\lvert s(0)\rvert^2$
-1	2	-1	0	$g\beta\gamma\beta_N(F_\mu/5)\frac{2}{5}\langle 1/r^3\rangle$
-1	-1	2	0	$g\beta\gamma\beta_N(F_\sigma/5)\frac{2}{5}\langle 1/r^3\rangle$
2	-1	-1	0	$g\beta\gamma\beta_N(F_\Pi/5)\frac{2}{5}\langle 1/r^3\rangle$
0	0	0	$-\frac{3}{2}$	$g\beta\gamma\beta_N(G_{\mu\sigma}/5)\frac{2}{5}\langle 1/r^3\rangle$

either nuclear level of m may go to either of those for $m+1$. If the change in the field direction is close to 0° or 180°, one pair of transitions will be almost inhibited; the spectrum arising in such a case we call *simple*. The spectra observed by Tinkham under his particular experimental conditions were all of this type. On the other hand, a spectrum with contributions from all transitions present to a significant extent we call *complex*. Clearly a substantial change in the direction of the effective magnetic field is necessary for excitation of such a spectrum. This requires that the *resultant field in the direction of the applied field H_0 and the transverse hyperfine field be comparable in magnitude.*

If we write $A_p{}^i$ for the hyperfine component, $(\mathbf{n}\cdot A_i\cdot\mathbf{n})$ along $\mathbf{n}$ and $|A_n{}^i|$ for the magnitude of the component normal to $\mathbf{n}$, two quantities $\epsilon_m{}^i$ and $\theta_m{}^i$ may be defined by

$$\epsilon_m{}^i=+[(A_p{}^i m+\gamma\beta_N H_0)^2+m^2|A_n{}^i|^2]^{\frac{1}{2}}$$
and
$$\tan\theta_m{}^i=m|A_n{}^i|/(mA_p{}^i+\gamma\beta_N H_0). \tag{18}$$

The nuclear energy levels will now be $E^i(m,+)=\frac{1}{2}\epsilon_m{}^i$ and $E^i(m,-)=-\frac{1}{2}\epsilon_m{}^i$. The relative probabilities of the transitions are given by

$$\begin{aligned}(m,+)\leftrightarrow(m+1,+)&=(m,-)\leftrightarrow(m+1,-)\\&=p_{m,m+1}{}^i=\cos^2[(\theta_m{}^i-\theta_{m+1}{}^i)/2]\\(m,+)\leftrightarrow(m+1,-)&=(m,-)\leftrightarrow(m+1,+)\\&=q_{m,m+1}{}^i=\sin^2[(\theta_m{}^i-\theta_{m+1}{}^i)/2].\end{aligned} \tag{19}$$

All these considerations apply to each of the 6 independent nuclei and the complete transition scheme may be summarized by writing down the expression:

$$2^{-6}\prod_{i=1}^{6}[p_{m,m+1}{}^i(x^{\frac{1}{2}r-}+x^{-\frac{1}{2}r-})+q_{m,m+1}{}^i(x^{\frac{1}{2}r+}+x^{-\frac{1}{2}r+})]. \tag{20}$$

where $r+=\epsilon_m{}^i+\epsilon_{m+1}{}^i$, $r-=\epsilon_m{}^i-\epsilon_{m+1}{}^i$. When this is expanded the exponents of x give the possible energy differences and the associated coefficients the relative intensities. Symmetry and the choice of applied field direction mercifully reduce the full number of 4^6 lines.

In the present series of experiments H has been directed in the [001], [100], and [110] directions. In each case it will be found that the four nuclei of types I and I′ are equivalent so far as their energy levels are concerned. In the same way the pair of type II nuclei are equivalent. With the magnetic field along the [001] axis we have

$$\begin{aligned}\epsilon_m{}^{\rm I}&=[(mA_{zz}{}^{\rm I}+\gamma\beta_N H_0)^2+m^2A_{yz}{}^{\rm I2}]^{\frac{1}{2}}\\\tan\theta_m{}^{\rm I}&=m|A_{yz}{}^{\rm I}|/(mA_{zz}{}^{\rm I}+\gamma\beta_N H_0)\\\epsilon_m{}^{\rm II}&=mA_{zz}{}^{\rm II}+\gamma\beta_N H_0\\\tan\theta_m{}^{\rm II}&=0.\end{aligned} \tag{21}$$

Only the type I and I′ nuclei contribute to the abnormality. The positions of the lines and their intensities are found from expansion of

$$2^{-6}[p_{m,m+1}{}^{\rm I}(x^{\frac{1}{2}R-}+x^{-\frac{1}{2}R-})+q_{m,m+1}{}^{\rm I}(x^{\frac{1}{2}R+}+x^{-\frac{1}{2}R+})]^4(x^{A_{zz}{}^{\rm II}}+x^{-A_{zz}{}^{\rm II}})^2, \tag{22}$$

where $R+=\epsilon_m{}^{\rm I}+\epsilon_{m+1}{}^{\rm I}$, $R-=\epsilon_m{}^{\rm I}-\epsilon_{m+1}{}^{\rm I}$.

There are $5\times5\times3=75$ distinct lines in the present case; there being, in fact, five levels of the set of four nuclei with all transitions allowed, while for the pair of Type II there are three levels and three admissible transitions. For comparison it should be noted that a completely simple spectrum has $5\times3=15$ lines. Exactly similar formulas hold for the [110] direction, but with $A_{yy}{}^{\rm I}$ and $A_{yy}{}^{\rm II}$ substituted for $A_{zz}{}^{\rm I}$ and $A_{zz}{}^{\rm II}$. The [100] direction is somewhat more involved and both sets of nuclei may have complex transitions. The relevant expressions are:

$$\epsilon_m{}^{\rm I}=\left[\left(\frac{A_{xx}{}^{\rm I}+A_{yy}{}^{\rm I}}{2}m+\gamma\beta_N H_0\right)+m^2\left(\frac{A_{xx}{}^{\rm I}-A_{yy}{}^{\rm I}}{2}\right)^2+\tfrac{1}{2}(A_{yz}{}^{\rm I})^2\right]^{\frac{1}{2}} \tag{23}$$

TABLE II. Type II.

A_{xx}	A_{yy}	A_{zz}	
2	-1	-1	$g\beta\gamma\beta_N(F/5)(1/R_{\rm II}^3)$
1	1	1	$g\beta\gamma\beta_N(f_s/5)(8\pi/3)\lvert s(0)\rvert^2$
-1	-1	2	$g\beta\gamma\beta_N(f_\mu/5)\frac{2}{5}\langle 1/r^3\rangle$
2	-1	-1	$g\beta\gamma\beta_N(f_\sigma/5)\frac{2}{5}\langle 1/r^3\rangle$
-1	2	-1	$g\beta\gamma\beta_N(f_\pi/5)\frac{2}{5}\langle 1/r^3\rangle$

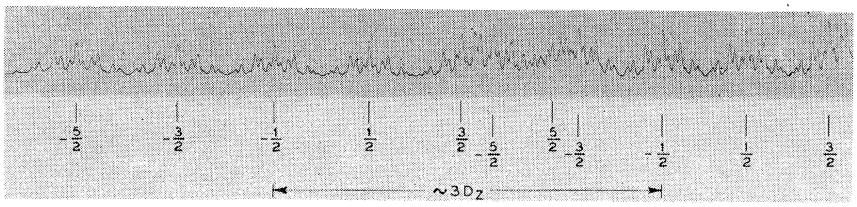

FIG. 3. A portion of the EPR spectrum of Mn^{++}:ZnF_2 observed at 23 kMc with $H_0 \| [001]$ and $T = 77°K$. (H_0 increases as one goes from left to right.) The magnetic quantum numbers belonging to the Mn^{55} hfs components of the electronic transition $M_s = -\frac{5}{2} \leftrightarrow M_s - 1 = -\frac{3}{2}$ are indicated in the upper row. Similarly the lower row of numbers identifies corresponding components in the $M_s = -\frac{3}{2} \leftrightarrow M_s - 1 = -\frac{1}{2}$ transition. The magnitude of the electronic fine structure splitting is $3D_z$. The separation of Mn^{55} hfs components is of order A^{55} and the super hfs due to the F^{19} nuclei is clearly visible on each Mn^{55} hfs component since $A^{19} < A^{55}$.

$$\tan\theta_m^{\mathrm{I}} = \frac{\{[(A_{xx}^{\mathrm{I}} - A_{yy}^{\mathrm{I}})/2]^2 + \frac{1}{2}(A_{yz})^2\}^{\frac{1}{2}}}{m[(A_{xx}^{\mathrm{I}} + A_{yy}^{\mathrm{I}})/2] + \gamma\beta_N H_0} \tag{24}$$

$$\epsilon_m^{\mathrm{II}} = \left[\left(\frac{A_{xx}^{\mathrm{II}} + A_{yy}^{\mathrm{II}}}{2} m + \gamma\beta_N H_0\right)^2 + \left(\frac{A_{xx}^{\mathrm{II}} - A_{yy}^{\mathrm{II}}}{2}\right)^2 m^2\right]^{\frac{1}{2}} \tag{25}$$

$$\tan\theta_m^{\mathrm{II}} = \frac{|A_{xx}^{\mathrm{II}} - A_{yy}^{\mathrm{II}}|/2}{[(A_{xx}^{\mathrm{II}} + A_{yy}^{\mathrm{II}})/2]m + \gamma\beta_N H_0} \tag{26}$$

$5 \times 5 \times 3 \times 3 = 225$ lines are possible in this spectrum, since all transitions are now allowed between the three levels of the pair.

OBSERVED SPECTRA AND ANALYSIS

K-Band Frequencies

The formalism given in the previous section predicts that the $(2S)(2I^{55}+1) = 30$ Mn^{55} hyperfine components of the EPR spectra normally expected, when transitions between electronic levels are induced such that $\Delta M_s = \pm 1$, have superimposed upon them an F^{19} hfs which need *not* be the same for each transition $M_s \leftrightarrow M_s - 1$. In particular, because of the presence of a large off-diagonal hfs interaction term (A_{yz}^{I}), and when for example, $M_s A_{zz}^{\mathrm{I}} \simeq \gamma^{19} H_0$, transitions in which $\Delta m_I^{19} = \pm 1$ as well as $\Delta m_I^{19} = 0$ will have comparable probability, resulting in a more complex spectrum.

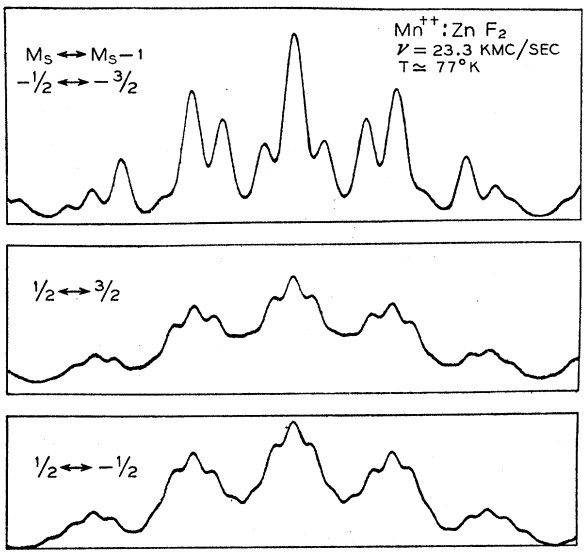

FIG. 4. The $M^{55} = +\frac{1}{2}$ hfs component of each of three electronic transitions in the EPR of Mn^{++}:ZnF_2 with $H_0 \| [001]$. The F^{19} hfs in the $-\frac{1}{2} \leftrightarrow -\frac{3}{2}$ transition resembles the spectrum observed by Tinkham at X-band frequencies while the others clearly do not.

$H_0 \| z$

To gain a point of view for further analysis we reproduce a portion of the spectra to k-band frequencies with $H_0 \| [001]$: (see Fig. 3). The notation used in identifying the transitions is given in the figure caption. Here the importance of the relative magnitudes of the crystal field splitting and that of the hyperfine interactions can be seen most clearly. Since $3D_z > A^{55}$ the Mn hfs components do not overlap sufficiently to obliterate the distinct shape of at least two of the six hfs components on each fine structure spacing. Similarly A^{55} is sufficiently larger than the A^{19}'s so that a negligible overlap of the "super hfs" on adjacent Mn^{55} hfs components exists.

In Fig. 4 we have reproduced a single Mn^{55} hfs component from each of the three electronic transitions with $H_0 \| [001]$. The top one corresponds to the transition $(-\frac{5}{2} \leftrightarrow -\frac{3}{2})$, the middle one $(-\frac{1}{2} \leftrightarrow \frac{1}{2})$, and the lower one $(\frac{1}{2} \leftrightarrow \frac{3}{2})$. The remaining two, $(\frac{3}{2} \leftrightarrow -\frac{1}{2})$ and $(+\frac{3}{2} \leftrightarrow \frac{5}{2})$ (not shown) are for all purposes identical in appearance with the first (or "simple") one. Each of the Mn^{55} hfs components for transitions emanating from the $M_s = +\frac{1}{2}$ level are "complex." The "complex" spectra cannot be fitted using Tinkham's theory by assuming any given set of values for A_z^{I} or A_z^{II}. The integrated intensities of every resolved Mn^{55} hfs components of each electronic transition $M_s \leftrightarrow M_{s-1}$ still satisfied the ratio predicted for $S = \frac{5}{2}$, namely 5:8:9:8:5.

$H_0 \| x, y$

Along [110] the spectra from the two nonequivalent sites no longer coincide, the field being in the x direction at one site and the y direction at the other. Since g is isotropic the observed spectra are further complicated by the fact that the smallness of D_x results in the x

spectrum appearing collapsed in the center of the y spectrum. However, D_y is sufficiently larger than D_x so that the outermost transitions are well resolved $[(-\frac{5}{2}\leftrightarrow-\frac{3}{2})$ and $(\frac{5}{2}\leftrightarrow\frac{3}{2})]$ and appear to be "simple." One such Mn^{55} hfs component is reproduced in Fig. 5. Thus, though "complex" spectra are predicted for the center transitions, the collapsed x spectrum prevents one from observing them.

$H_0\|a$

With the field parallel to [100] the two sites again become equivalent and precise measurement of the F^{19} hfs for this case makes possible a determination of the quantities A_{xx}^{I} and A_{xx}^{II}. This spectrum was not observed by Tinkham and contributed to his mistaken belief that $A_s^{I}=1.2A_s^{II}$. That this is not so is seen most clearly in the comparison of a portion of the spectrum with $H_0\|c$ with that of one with $H_0\|\bar{a}$, as is given in Fig. 5. The relative magnitudes of the components of A^{I} and A^{II} are practically interchanged in these two spectra.

54 KMC MEASUREMENTS: $H_0\|[001]$

Since the experimental arrangement used at 54 kMc was inherently less sensitive than the 23 kMc apparatus it was necessary to use phase-sensitive detection with small field modulation. As a result the observations correspond to the *derivative* of the expected spectra. In Fig. 6 we have reproduced a single Mn^{55} component from each of the electronic transitions; $(\frac{1}{2}\leftrightarrow-\frac{1}{2})$, $(\frac{3}{2}\leftrightarrow\frac{1}{2})$, and $(\frac{5}{2}\leftrightarrow\frac{3}{2})$. The corresponding components of the remaining two transitions are, in appearance, identical with the $(\frac{1}{2}\leftrightarrow-\frac{1}{2})$ transition. The $(\frac{1}{2}\leftrightarrow-\frac{1}{2})$

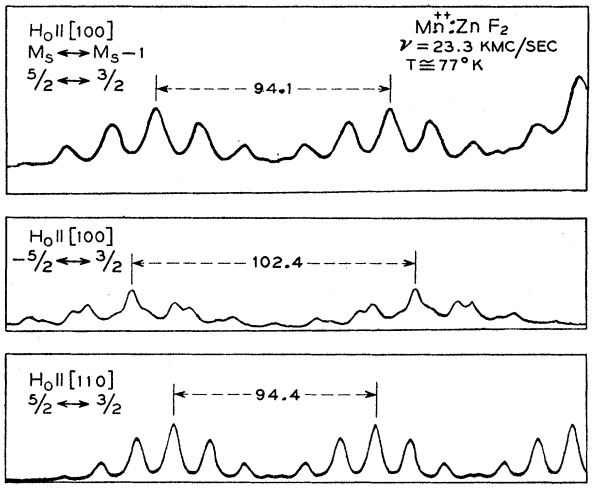

FIG. 5. Portions of the EPR spectrum of Mn:ZnF_2 with H_0[100] and H_0[110]. Separation of the centers of successive Mn^{55} components are given in oersteds. The "normal" spectrum observed with H_0[100] in the transition $(-\frac{5}{2}\leftrightarrow-\frac{3}{2})$ should be compared with the "normal" spectrum in the top of Fig. 4. The relative magnitudes of A^{I} and A^{II} are approximately interchanged in these two spectra.

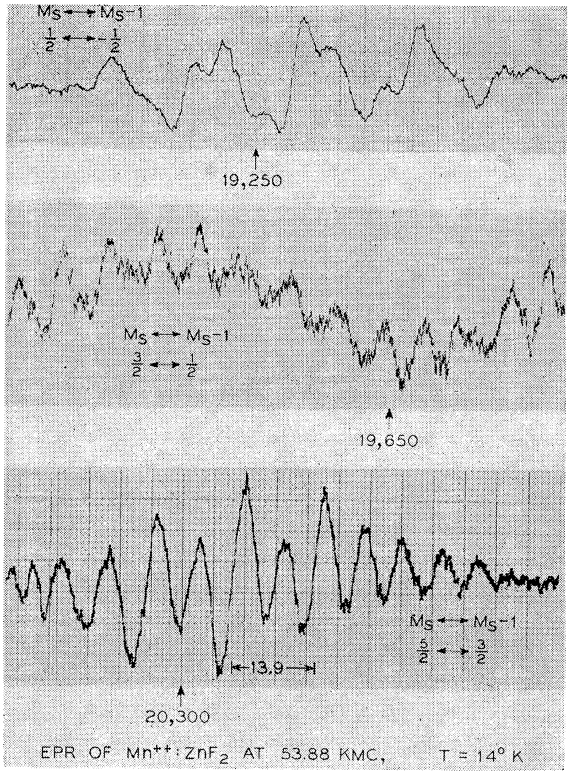

FIG. 6. Portions of the EPR spectrum of Mn^{++}:ZnF_2 at 54 kMc with $H_0\|[001]$ and $T=14°K$. The derivative of each of three hfs components is given for three distinct electronic transitions. The complexity in the spectra at 54 kMc is present in transitions which have the $M_s=+\frac{3}{2}$ level in common whereas for the same direction at 23 kMc the complexity was common to the transitions which had the $M_s=+\frac{1}{2}$ level in common. It is to be noticed that the two complex spectra are different at these frequencies both from each other and from the complex spectra observed at K band frequencies. The field separation indicated on the lowest transition in the figure corresponds to certain predicted values of the F^{19} hfs components for this electronic transition. Approximate values of H_0 are indicated on each recorded trace. Field inhomogeneities at these large applied fields unfortunately increase the line widths of each F^{19} hfs component.

spectra is simple (the recorded shape may be compared directly with that given in reference 1). A broadening of each line exists due to field inhomogeneities at these high fields.

As predicted by the theory and assuming the values of the relevant parameters determined from the k-band measurements the complex transitions are those that originate, or terminate at the $M_s=+\frac{3}{2}$ level. In addition, it is predicted that the two complex transitions should appear to be quite different. These qualitative features are reproduced in our observed spectra with the $(\frac{3}{2}\leftrightarrow\frac{1}{2})$ component having the more "complex" character, and represent in particular a confirmation of the large value chosen for A_{yz}^{I}.

ANALYSIS OF THE K-BAND DATA

The transitions which have been analyzed in some detail are the $-\frac{3}{2}\leftrightarrow-\frac{1}{2}$, $-\frac{1}{2}\leftrightarrow\frac{1}{2}$, and $\frac{1}{2}\leftrightarrow\frac{3}{2}$ cases in

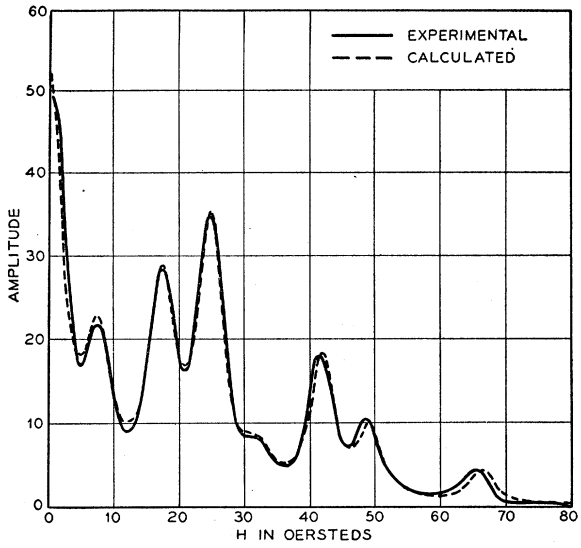

FIG. 7. A comparison of experiment and theory for the "simple" F^{19} hfs observed at K band on the electronic transition $M_s=-\frac{1}{2}\leftrightarrow M_s=-\frac{3}{2}$, when $H_0\|[001]$. The parameters used are those given in Tables III and IV. The curves are normalized to have equal areas. Failure to correct completely for the nonlinearity of the field sweep accounts for the progressive deviation of the two curves.

the [001] direction, of which the first is "simple" and the latter pair "complex"; the $-\frac{5}{2}\leftrightarrow-\frac{3}{2}$ transition in the [100] and [110] directions, both being "simple." Each of these cases had the advantage of being free from overlap by neighboring transitions.

From the appearance or nonappearance of "complex" spectra and an approximate visual analysis of the various transitions a rough estimate was first made of $A_{yz}{}^{\mathrm{I}}$. On the basis of this it was considered that the $-\frac{3}{2}\leftrightarrow-\frac{1}{2}$ transition in the [001] direction was completely "simple." This was verified with the final values of the A's from which

$$\tfrac{1}{2}(\theta_{-\frac{1}{2}}{}^{\mathrm{I}}-\theta_{-\frac{1}{2}}{}^{\mathrm{I}})$$

is found to be about 2° ($\sin^2 2°\sim 0.0001$). We therefore take

$$\begin{aligned}|\epsilon_{-\frac{1}{2}}{}^{\mathrm{I}}-\epsilon_{-\frac{3}{2}}{}^{\mathrm{I}}|&=[(A_{zz}{}^{\mathrm{I}})^2+(A_{yz}{}^{\mathrm{I}})^2]^{\frac{1}{2}}=A_{zz}{}^{\mathrm{I}\prime}\\ |\epsilon_{-\frac{1}{2}}{}^{\mathrm{II}}-\epsilon_{-\frac{3}{2}}{}^{\mathrm{II}}|&=A_{zz}{}^{\mathrm{II}}\end{aligned}\qquad(27)$$

and use the intensities for the "simple" case. $A_{zz}{}^{\mathrm{I}\prime}$, $A_{zz}{}^{\mathrm{II}}$ and a line width parameter were then found by the following procedure. The spectrum as observed was supposed to consist of a sum of Gaussians or of Lorentzians, centered at the predicted lines and with the correct relative intensities. The absolute intensity was fixed by requiring the area under the predicted and observed spectra to be the same. The integral of the squared deviation of predicted and observed spectra was evaluated over the spectrum. This quantity was then minimized with respect to $A_{zz}{}^{\mathrm{I}\prime}$, $A_{zz}{}^{\mathrm{II}}$, and the line width parameter by trial and error. This analysis was carried out on an IBM 704 computer by Miss M. C. Gray. It became apparent very quickly that the Lorentzian lines gave a substantially better fit than did the Gaussians, the difference amounting to a factor of two or three in the least attainable value for the deviation integral. We, therefore confined the analysis to Lorentzian lines. A similar analysis was carried through for the other "simple" lines: the $-\frac{5}{2}\leftrightarrow-\frac{3}{2}$ transitions in the [100] and [110] directions. The first of these gives values of $[(A_{yy}{}^{\mathrm{I}})^2+(A_{yz}{}^{\mathrm{I}})^2]^{\frac{1}{2}}$ and $A_{yy}{}^{\mathrm{II}}$,

TABLE III. The F^{19} hfs interaction constants derived from the EPR of Mn^{++}:ZnF_2. The choice of the principal axes of the hfs interaction tensor, the methods used in evaluating the constants from the K-band data, and the errors in the derived quantities are discussed in the text. The units in the first row are electron gauss, and 10^{-4} cm^{-1} in the second.

$A_{xx}{}^{\mathrm{I}}$	$A_{yy}{}^{\mathrm{I}}$	$A_{zz}{}^{\mathrm{I}}$	$A_{yz}{}^{\mathrm{I}}$	$A_{xx}{}^{\mathrm{II}}$	$A_{yy}{}^{\mathrm{II}}$	$A_{zz}{}^{\mathrm{II}}$
16.63	16.73	19.13	4.7	24.97	14.38	13.80
11.81	15.57	17.83	4.4	23.34	13.44	12.90

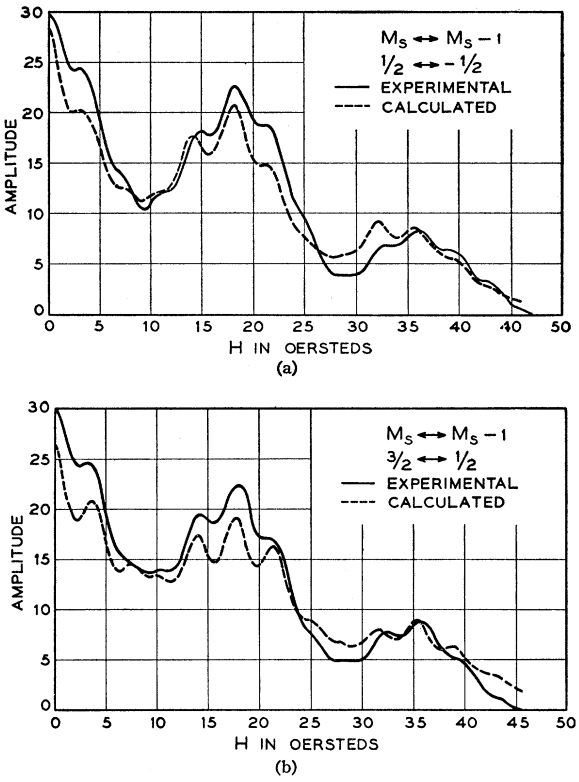

FIG. 8. A comparison of experiment and theory for the "coms plex" F^{19} hfs observed at K band on the electronic transition $M_s=+\frac{1}{2}\leftrightarrow M_s-1=-\frac{1}{2}$ and $M_s=\frac{3}{2}\leftrightarrow M_s=-\frac{1}{2}$ with $H_0\|[001]$. The parameters used are those given in Tables III and IV and $\gamma=13.5°$. The curves are normalized to have equal area. The somewhat less satisfactory agreement resulted in part from the difficulty in establishing the tailends of the experimental spectra due to overlap with the adjacent structure of a neighboring Mn^{55} hfs component. It also appears that choosing a slightly large value of the line width parameter than is obtained in the "simple" case would improve the agreement, though there is no *a priori* reason for doing so.

while the second yields $[\frac{1}{2}(A_{xx}^{I2}+A_{yy}^{I2}+A_{yz}^{I2})]^{\frac{1}{2}}$ and $[\frac{1}{2}(A_{xx}^{I2}+A_{yy}^{I2})]^{\frac{1}{2}}$. The quality of the fit was about the same for all three directions and may be assessed roughly in the following way: we have calculated

$$I=\int_{-H_{max}}^{H_{max}}[f(x)-f_0(x)]^2dx,$$

where $H_{\max}$ is the effective end of the spectrum, $f(x)$ is the observed, and $f_0(x)$ the calculated intensity. Then, $(H/2H_{\max})^{\frac{1}{2}}[1/f(0)]\sim 0.02$ for all three cases, with $f(0)$ being the height of the central peak.

Using the values of A_{zz}^{I}, A_{zz}^{I}, and the line width parameter obtained from the "simple," $-\frac{3}{2}\leftrightarrow-\frac{1}{2}$, transition, intensities were then calculated for the "complex," $-\frac{1}{2}\leftrightarrow\frac{1}{2}$, and $\frac{1}{2}\leftrightarrow\frac{3}{2}$ transitions in the [001] direction. The procedure was to assume various values for γ where $\tan\gamma=A_{yz}^{I}/A_{zz}^{I}$ and then to calculate the ϵ_m^{I} and θ_m^{I} from Eqs. (23) and (24) and use these values to find the positions and intensities of the lines. A spectrum was then synthesized using a superposition of Lorentzians of the same width as in the "simple" spectrum. These spectra were then compared visually with the observed spectra. The best fit is by no means as good as that found for the "simple" spectrum, but the value of γ ($\gamma=13.5°$) giving the best agreement is very nearly the same for the two "complex" cases. The estimate of γ, we would judge, is good to $\pm 1.5°$. [Compare Fig. 9 with Figs. 8(a), (b).]

TABLE IV. The line widths (half-widths at half-power) of the F^{19} hfs components of the EPR of Mn:ZnF_2 as measured at K-band frequencies and at 77°K. As explained in the text these are computational best fits when the line shape is assumed to be Lorentzian.

Direction of H_0	$(\delta H)_{\frac{1}{2}}$ oe
[001]:z	1.80±0.05
[110]:y	2.40±0.05
[100]:xy	2.30±0.05

The parameters measured in the EPR experiment are collected in Table III. Systematic error analysis was not obtained from our machine computation but an assignment of error may be given as follows. All of the measured quantities suffer an error of about 1% due to field calibration and correction for nonlinearity in the field sweep. Considering, in addition, the widths of the observed lines, it is reasonable to assign a conservative error of 1.5% to the A_{zz}'s and 2% to the A_{xx}'s and A_{yy}'s. An uncertainty of approximately 10% exists in the determination of A_{yz}, the error being directly related to the error in γ.

The line width parameters obtained by the above procedures are given in Table IV. It is not clear to the authors why a Lorentzian, rather than a Gaussian, shape should provide a better fit to the data. One would presume the origin of the line width to be the dipole

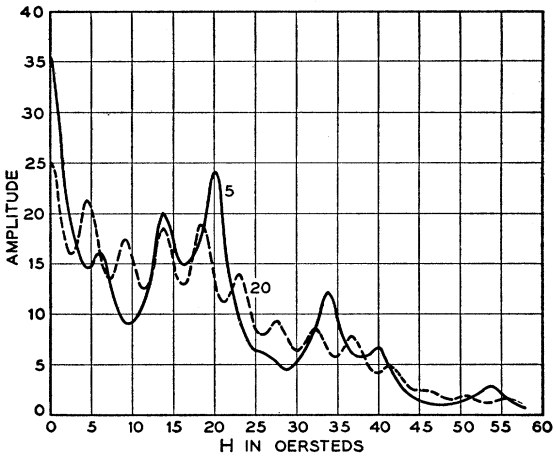

FIG. 9. The theoretical hfs expected for the transition $M_s=+\frac{1}{2}\leftrightarrow M_s=-\frac{1}{2}$ for two different values of γ; $\gamma=5°$ and $\gamma=20°$. [See Fig. 8(a) and caption.] It can be seen that the "complex" spectra changes character rather rapidly as a function of γ.

fields of the other than 6 nearest F^{19} neighbors to a given Mn^{++} and the magnitude of the line width is consistent with this assumption. Such a distribution of randomly oriented dipoles would be expected to lead to a Gaussian line shape.

The isotropic and anisotropic constants that may be computed from the phenomenological constants of Table III are given in Table V. Several points should be made concerning the computation and form of presentation of these parameters. For the type II parameters one may straightforwardly obtain A_s, A_D+A_σ, and A_π, whereas for the Type II case to obtain A_D+A_s and A_σ one must assume a knowledge of β and α. Now, if one uses the data of Baur or Stout for either the ZnF_2 or MnF_2 lattice, β may be seen to vary by only a few degrees. We have arbitrarily taken β to be 38.6°. The quantity $A_D^{I}+A_\sigma^{I}$ is given by

$$A_D^{I}+A_\sigma^{I}=-\frac{2A_{yz}^{I}\sin(\alpha+\beta)+(A_{zz}^{I}-A_{yy}^{I})\cos(\alpha+\beta)}{3\cos(\alpha-\beta)}. \quad (28)$$

Using the experimentally determined values of A_{yz}^{I}, A_{zz}^{I}, and A_{yy}^{I} it was found that $A_D^{I}+A_\sigma^{I}$ was remarkably insensitive to the choice of α, there being a variation of less than 4% in $A_D^{I}+A_\sigma^{I}$ as α is varied from 0° to 60°. Hence α was arbitrarily chosen to be equal

TABLE V. The isotropic and anisotropic constants of the F^{19} hfs from the EPR of Mn^{++}:ZnF_2 that are derived from the phenomenological constants of Table III using the theory given in the text. The units are electron gauss.

	A_s	(A_D+A_σ)	A_π
Type I	+16.16±0.17	+3.23±0.32	−0.15±0.22
Type II	+17.72±0.20	+3.72±0.18	+0.19±0.12

to β. Using this value of $A_D^{\rm I}+A_\sigma^{\rm I}$ a value of $A_\pi^{\rm I}$ was determined. The error in both of these quantities reflects the relatively large error in $A_{yz}^{\rm I}$. That this same problem does not enter the determination of the corresponding type II quantities is a result of $A_{yz}^{\rm II}$ being identically zero.

The authors have chosen not to separate A_D and A_σ in the tables for, if one does, certain assumptions must then be made concerning inter-ion separation and the distribution of spin magnetization. Reasonable assumptions concerning bond lengths for the Mn^{++} in ZnF_2 (say $r_{\rm I}\cong r_{\rm II}=2.10\times10^{-8}$ cm) may be made and if one assumes all the Mn^{++} spin magnetization to be contained in a sphere of radius $R<2.10\times10^{-8}$ cm [i.e., $F=5$ in Eq. (12)] then $A_D^{\rm I}\cong A_D^{\rm II}=2.9$ and $A_\sigma^{\rm I}=+0.4$ and $A_\sigma^{\rm II}=+0.8$ (all in units of electron gauss). The experiments clearly indicate then that both the isotropic and anisotropic contributions to the hyperfine interaction that are not of dipolar origin are different for the distinct F^- sites. Considering the relative magnitudes of $A_D^{\rm I}$ and $A_\sigma^{\rm I}$ one can see why the quantity $A_D^{\rm I}+A_\sigma^{\rm I}$ is insensitive to variations in the choice of α in region of $\alpha\simeq\beta$.

COMPARISON OF THE EPR AND NMR EXPERIMENTAL RESULTS

In this section we compare the experimental results of the EPR of Mn^{++}:ZnF_2 (this work) and the NMR of F^{19} in MnF_2.[5,6,7,16] The justification for making such a comparison rests on the relative structural isomorphism of the crystals and the belief in the identity of the local Mn^{++} and F^- environments in the two crystals. Since this, at best, is a good approximation the fortuitous nature of any particular agreement should be as readily recognized from the outset as are the limits of experimental uncertainties in the measured parameters.

The NMR of F^{19} in Paramagnetic and Antiferromagnetic MnF_2

An analysis of the NMR experiments was originally given in terms of the F^{19} interaction constants used by Tinkham. It is clear from our work that this point bears re-examination.

The time-independent part of the Hamiltonian that describes the interaction of the nth F^{19} nuclear moment with the various effective magnetic fields may be written as

$$H_n=+\gamma\beta_N\hbar\mathbf{I}\cdot{}_n\left[\mathbf{H}_0+\frac{1}{\gamma\beta_N\hbar}\left(\sum_k^3 A^{kn}\cdot\langle\mathbf{S}^k\rangle+\sum_{d\neq k}^N D^{dn}\cdot\langle\mathbf{S}^d\rangle\right)\right] \quad (29)$$

where $\langle\mathbf{S}^k\rangle$ is the time average value of the kth electron spin momentum. The respective terms in the square bracket represent the applied field, the effective field produced by the hyperfine interaction with the three neighboring Mn^{++} spin moments, including that part which is of dipole origin, and the effective dipole field resulting from all but the three nearest Mn^{++} spin moments in the crystal. This last term is, of course, shape-dependent. The components of the D tensor for the MnF_2 lattice have been computed elsewhere.[7]

The grouping of the nearest-neighbor dipole field with the hyperfine terms is proper for two reasons. First, the measured A's are then formally identical with the corresponding interaction constants derived from EPR measurements in the dilute material. Furthermore, there are some approximations to be made if one is to separate the dipole interaction from the remaining interactions which have the same transformation properties since the magnetic cloud of d electrons partially overlap the F^{19} position. Our grouping allows for a phenomenological comparison without explicit assumptions concerning augmentation and orientation of p-electron orbitals and d-electron radial distributions.

It may be shown that for the NMR experiments in either the paramagnetic or antiferromagnetic states, the observed effects of the hyperfine tensor are such that it may be treated as if it had only diagonal components, with principal axes along the x, y, and z directions. To see this let us write $(-\gamma^{19}\hbar)$ times the effective hyperfine field in matrix product form

$$\left[\begin{vmatrix} A_{xx}^{\rm I} & 0 & 0 \\ 0 & A_{yy}^{\rm I} & A_{yz}^{\rm I} \\ 0 & A_{yz}^{\rm I} & A_{zz}^{\rm I} \end{vmatrix}\begin{vmatrix}\langle S_x^{\rm I}\rangle\\ \langle S_y^{\rm I}\rangle\\ \langle S_z^{\rm I}\rangle\end{vmatrix}+\begin{vmatrix} A_{xx}^{\rm I} & 0 & 0 \\ 0 & A_{yy}^{\rm I} & -A_{yz}^{\rm I} \\ 0 & -A_{yz}^{\rm I} & A_{zz}^{\rm I} \end{vmatrix}\begin{vmatrix}\langle S_x^{\rm I}\rangle\\ \langle S_y^{\rm I}\rangle\\ \langle S_z^{\rm I}\rangle\end{vmatrix}+\begin{vmatrix} A_{yy}^{\rm II} & 0 & 0 \\ 0 & A_{xx}^{\rm II} & 0 \\ 0 & 0 & A_{zz}^{\rm II} \end{vmatrix}\begin{vmatrix}\langle S_x^{\rm II}\rangle\\ \langle S_y^{\rm II}\rangle\\ \langle S_z^{\rm II}\rangle\end{vmatrix}\right]$$

where we have used the fact $A_{ii}^{\rm I}=A_{ii}^{\rm I'}$ and $A_{yz}^{\rm I}=-A_{yz}^{\rm I'}$. (The reordering of the xx and yy components of the $A^{\rm II}$ tensor accounts conveniently for the 90° rotation about the c axes of the octahedron of F^- ions in going from one nonequivalent site to the next.) Also $\langle S_i^{\rm I}\rangle=\langle S_i^{\rm I'}\rangle$.

Since the paramagnetic and antiferromagnetic states are distinguished only by the fact that in one $\langle S_z^{\rm I}\rangle=\langle S_z^{\rm II}\rangle$ whereas in the other $\langle S_z^{\rm I}\rangle=-\langle S_z^{\rm II}\rangle$ it is clear that the contributions for the $A_{yz}^{\rm I}$ terms vanish in either case.

If one assumes that $\langle S\rangle_T$ can be obtained from the measured susceptibility at temperature T in the paramag-

[16] J. L. Davis and V. Jaccarino (unpublished). A precise redetermination of the F^{19} hfs constants in *paramagnetic* MnF_2 was made at fields of 14 kilogauss and at $T=77$°K. Under these conditions all lines are clearly resolved. The results agreed with the earlier measurements (see reference 5) within the experimental errors previously given.

netic state the relevant parameters that may be measured are $2A_{zz}^{I}+A_{zz}^{II}$, $2A_{xx}^{I}+A_{yy}^{II}$, and $2A_{yy}^{I}+A_{xx}^{II}$. The situation in the antiferromagnetic state is somewhat more involved. The quantity actually measured, say at $T=0°K$, is $(2A_{zz}^{I}-A_{zz}^{II})\langle S_z\rangle_0$. However, even at $T=0°K$, it is not expected that $\langle S_z\rangle_0=\frac{5}{2}$ but that zero-point vibrations in the spin-wave spectrum will make $\langle S_z\rangle<\frac{5}{2}$. According to spin-wave theory $\langle S_z\rangle_0$ will be decreased by 3% from its maximum value, whereas a perturbation expansion[7] has shown the deviation from $\frac{5}{2}$ to be only 1.6%. A precise measurement of $\langle S_z\rangle_0$ would contribute to the elucidation of our problem —not to mention the importance of this quantity in the understanding of the ground state of the antiferromagnet.

COMPARISON OF THE F^{19} hfs INTERACTION CONSTANTS

For comparison purposes we have collected the NMR measurements and the corresponding combinations of the EPR measurements in Table II. The principal uncertainty in the hfs constants derived from the NMR measurements in the paramagnetic state is the experimental error in the *absolute* value of the spin susceptibility. This error is at least 1%. If one considers the ratio of quantities [e.g. $(2A_{yy}^{I}+A_{xx}^{II})/(2A_{xx}^{I}+A_{zz}^{II})$] this uncertainty disappears for the NMR measurements at the expense of an additional statistical error arising in the same ratio of the EPR-derived hfs constants. In the column headed "$2A_s^{I}+A_s^{II}$" is one-third of the sum of the quantities in the previous three columns. Quite properly this is also a model-independent, phenomenological, quantity. It assumes nothing concerning augmentation or bond directions and represents only a particular weighting of the two separate isotropic portions of the hyperfine interaction. *Within the experimental errors of both measurements, there is very good agreement, perhaps fortuitously so.* Again, the agreement in the comparison of the NMR results in the antiferromagnetic state and the EPR derived quantities is, though somewhat marginally, within experimental error if one assumes $\langle S\rangle_0$ to have a value in the range of that predicted by perturbation theory or spin wave theory. (See Table VII.)

That there should be agreement within a very few percent is not completely obvious when one considers the environment of a F^- ion in the two structures. In the dilute crystal the important F^- ions are surrounded by two Zn^{++} ions and one Mn^{++} ion as distinct from MnF_2 where all of the neighbors are Mn^{++}. The relevant structural parameters as determined by Stout and by Baur[8] are given in Table VI. Since small, but possibly finite, differences exist in the relevant cation-anion spacings in the two lattices, one may wonder if the Mn-F spacing in the ZnF_2 lattice is that characteristic of either lattice or intermediate between the two.

TABLE VI. The lattice parameters for the MnF_2 and ZnF_2 lattices, as determined at room temperature by Stout and Reed and by Baur (see reference 8).

		u	Type I Bond (4)	Type II Bond (2)
Stout	MnF_2	0.310±0.003	2.110 A	2.137 A
	ZnF_2	0.307±0.003	2.026	2.042
Baur	MnF_2	0.305±0.002	2.132	2.102
	ZnF_2	0.303±0.002	2.043	2.015

Fortunately, the difference in lattice parameters is small and, from the good agreement found, one can draw certain conclusions: (1) the hyperfine interactions are localized to nearest neighbors to a high approximation; (2) whatever is the proper physical description of the origin of the hyperfine interaction, information concerning the angular dependence and strength of the interaction can be obtained either by NMR in the dense magnetic crystal or EPR of the appropriate magnetic impurity in the host isomorphic diamagnetic crystal, assuming one does exist. One might hesitate to conclude what the environmental effects on the hfs interaction would be for ions manifestly foreign to the lattice (e.g., F^{19} hfs in Mn:CaF_2 or Mn:AlF_3) where considerations of size and/or valence state would alter the distribution of magnetic electrons at distances comparable to the anion-cation separation; (3) both NMR and EPR are complementary techniques insofar as hfs information is concerned and the demands of the problem would dictate which is most favorable. It might be instructive to pursue NMR in less dense paramagnetic materials which would provide data that is more readily comparable with that obtained from EPR measurements.

TABLE VII. A comparison of the F^{19} hfs interaction constants as derived from the F^{19} NMR of MnF_2 and the EPR of Mn^{++}:Z_nF_2. (The units are electron gauss.) The constants derived from the NMR measurements in the paramagnetic state suffer from an error of at least one percent caused by the uncertainty in the absolute value of the spin susceptibility. The fact that the measured quantities $2A_s^{I}+A_s^{II}$ agree so closely, combined with the rapid dependence expected for A_s with Mn-F separation, lends support to the belief that the local environment (bond distances, angles) of a Mn^{++} ion in ZnF_2 more closely resembles that of the MnF_2 lattice rather than the host lattice.

	Paramagnetic state				Antiferromagnetic state
	$2A_{xx}^{I}+A_{yy}^{II}$	$2A_{yy}^{I}+A_{xx}^{II}$	$2A_{zz}^{I}+A_{zz}^{II}$	$2A_s^{I}+A_s^{II}$	$2A_{zz}^{I}-A_{zz}^{II}$
EPR; $Mn^{++}ZnF_2$	$39.6_4\pm0.7_9$	$58.4_3\pm1.1_6$	$52.0_6\pm0.7_7$	$50.0_4\pm0.4_0$	$24.4_6\pm0.7_7$
NMR; MnF_2	$40.6_8\pm0.4_1$	$58.1_5+0.5_8$	$52.4_9\pm0.5_2$	$50.4_4\pm0.5_0$	23.0_9; $\langle S\rangle_0=\frac{5}{2}$ 23.4_6; $\langle S\rangle_0=2.460$ 23.7_9; $\langle S\rangle_0=2.425$

THE Mn^{55} hfs

Determination of the hfs Constants

The hfs of Mn^{55} on the EPR of Mn^{++} has been extensively studied beginning with the work of Bleaney and Ingram.[17] A theory of the origin of the unexpectedly large observed hfs was first given by Abragam and Pryce.[18,19] A more satisfying theory (in respect to numerical agreement with experiment) has been proposed by Heine[20] which accounts for the magnitude of the hfs both in the divalent ion and in the neutral atom by considering the effects of exchange polarization by the d electrons on the inner s electrons.

Since a slight anisotropy was observed in the Mn^{55} hfs it is necessary to describe the interaction by adding to the spin Hamiltonian a term of the form

$$\mathcal{H}^{55}=AI_zS_z+B(I_xS_x+I_yS_y). \tag{30}$$

As a result of (30) the field for resonance for the electronic transition $M_S \leftrightarrow M_S-1$, for which $\Delta M_I=0$, is changed from (1) by an amount

$$-KM_I-\frac{B^2}{4H_0}\left(\frac{A^2+K^2}{K^2}\right)[I(I+1)-M_I^2] -\frac{B^2}{2H_0}\frac{A}{K}[M_I(2M_S-1)]$$

where, since g is isotropic, $K^2=A^2\cos^2\theta+B^2\sin^2\theta$ and θ is the angle made by the field and the z axis.

Careful measurements of first and second differences of the Mn^{55} hfs intervals, at K band, with $H_0\|[001]$, [110], and [100] produced the following results:

$$\begin{aligned} A^{55}&=-97.1\pm0.3g \\ B^{55}&=-98.8\pm0.5g. \end{aligned} \tag{31}$$

These values lie outside the experimental error of the value obtained by Tinkham[1] in which he assumed the hfs interaction to be isotropic. The value he obtained was $A^{55}=(103\pm3)g$.

Determination of the Sublattice Magnetization at 0°K

$M(0)$, *in Antiferromagnetic* MnF_2

Since the hfs interaction of Mn^{55} in MnF_2 should be identical with that of Mn^{55} in $Mn:ZnF_2$ our measurements of A^{55} may be combined with recent nuclear spin specific heat measurements of MnF_2 at very low temperatures by Cooke and Edmonds[21] to determine $M(0)$.

In antiferromagnetic MnF_2 the effect of the hfs interaction is accounted for by the addition to the Hamiltonian of the term

$$\sum_i^{N/2} AI_z{}^i\langle S_z{}^i\rangle \tag{32}$$

since the z direction is the direction of antiferromagnetic alignment and where $\langle S_z\rangle$ is the averaged value of the electron spin polarization. The magnetization of a sublattice would then be given by

$$M=(N/2)g\beta\langle S_z{}^i\rangle.$$

Expression (32) is not exact for we have not accounted for the field $D_z{}^i\langle S_z{}^i\rangle$ resulting from all of the remaining Mn^{++} dipoles when considering the hfs interaction at the ith site.

Similarly the F^{19} hfs and the Mn^{++} dipole fields at the F^- sites contribute to the F^{19} spin specific heat. Using our values for $A_z{}^{55}$, $2A_{zz}{}^{I}-A_z{}^{II}$, and the appropriate dipole fields we may, with Cooke and Edmonds data, calculate the magnetization of a sublattice. The value so obtained is

$$M(0)_{\text{exp}}/M(0)_{s=\frac{5}{2}}=(101\pm2)\% \tag{33}$$

where all of the error quoted resides in the specific heat measurements. Since $\langle S_z\rangle$ must be $\leq\frac{5}{2}$ it is perhaps more instructive to say that the deviation of the magnetization from saturation does not appear to exceed one percent.

A fuller discussion of these results is given in reference 7.

It should be noticed that the F^{19} NMR and EPR results are consistent with this value of $\langle S_z\rangle$ whereas the old experiments[1] necessitated choosing a 10% spin deviation at $T=0$ to bring the results into coincidence.

CONCLUSIONS

A detailed experimental treatment and phenomenological description has been given of the F^{19} hfs interaction in the EPR of Mn^{++} as a dilute substitutional impurity in ZnF_2. Certain features of EPR experiments in systems in which the central ion magnetization overlaps the positions of the nuclei of the surrounding ions to an extent such that a resolvable hfs exists have been elucidated, to wit:

(1) For other than cubically octahedral environment there will *not* exist a coordinate system in which the hfs interaction for *all* of the ligand nuclei is simultaneously diagonal.

(2) The presence of large off-diagonal components of the hfs interaction in this case will make possible transitions which appear to have $\Delta m_i=\pm1$ as well as $\Delta m_i=0$ selection rules. This will happen whenever the effective resultant fields at the nucleus, parallel and perpendicular to the external field, are comparable in magnitude and either one changes appreciably as a result of an electronic transition.

[17] B. Bleaney and D. J. E. Ingram, Proc. Roy. Soc. (London) **A265**, 336 (1951).
[18] A. Abragam and M. H. L. Pryce, Proc. Roy. Soc. (London) **A205**, 135 (1951).
[19] Abragam, Horowitz, and Pryce, Proc. Roy. Soc. (London) **A230**, 169 (1955).
[20] V. Heine, Phys. Rev. **107**, 1002 (1957).
[21] A. H. Cooke and D. T. Edmonds, Proc. Phys. Soc. (London) **71**, 517 (1958).

(3) Such complex spectra may occur in cubically octahedral environments as well when the external field is not along a direction corresponding to a principal axis of the hfs tensor and if the hfs is anisotropic.

(4) This critical re-examination of the $Mn^{++}ZnF_2$ system should be extended to that of Fe^{++} and Co^{++} before the F^{19} hfs may be interpreted for similar effects which will be present in these two cases.[1]

Futhermore any "first principles" calculation of the magnitudes of the respective F^{19} hfs constants must, for other than the isotropic contribution, take into account the low symmetry about the central ion in the ZnF_2 host lattice.

We have demonstrated that there exists very good agreement between the measurements made herein and shifts of the NMR of F^{19} observed in paramagnetic and an antiferromagnetic MnF_2.

ACKNOWLEDGMENTS

The authors are indebted to M. Tinkham, T. P. Das, F. Keffer, and W. Marshall for discussions and preprints of their work.

PHYSICAL REVIEW VOLUME 117, NUMBER 5 MARCH 1, 1960

Pyroelectricity, Internal Domains, and Interface Charges in Triglycine Sulfate

A. G. CHYNOWETH
Bell Telephone Laboratories, Murray Hill, New Jersey
(Received September 28, 1959)

Using the dynamic pyroelectric technique, the spontaneous polarization of triglycine sulfate has been determined between the Curie point and −140°C. No evidence of any phase transitions over this temperature range was found (other than the Curie point). The polarization could still be reversed by an applied field, though slowly, at the lowest temperatures attained. In the paraelectric region above the Curie point, the pyroelectric behavior shows some deviations at low applied fields from the predictions of Devonshire's theory. The cause of these deviations is not known but they may be due to nonuniform conditions, either mechanical or electrical, in the crystal.

With no field applied to the crystal, pyroelectric signals can be generated temporarily above the Curie point. These are ascribed mainly to polarizations induced by the compensation charges while they last, which accumulate around residual domains that cannot be removed by the poling field at room temperature. These residual domains have been delineated using powder pattern and etching techniques and are revealed as long thin domains, pointed at both ends and lying along the ferroelectric direction, either in the interior of the crystal or intercepting the surfaces. The causes of these persistent domains are not known.

It is found that on cooling a crystal through the Curie point, there is a strong tendency for it to repolarize with the same polarity it had previously. This phenomenon is ascribed to the presence of ferroelectrically inactive surface layers giving rise to interface charges.

INTRODUCTION

THIS paper is concerned with a pyroelectric investigation of the ferroelectric crystal triglycine sulfate, using techniques that have been described in detail elsewhere.[1–3] The spontaneous polarization has been determined down to −140°C and the pyroelectric properties of the crystal in the paraelectric region above the Curie point have been studied and compared with the predictions of Devonshire's theory.[4] In addition, small pyroelectric signals have been observed above the Curie point when no external field is applied and the probable origins of these are discussed in some detail. Furthermore, evidence for surface layers is found from studies of the repolarizing of the crystals on cooling through the Curie point.

EXPERIMENTAL

Thin slices cleaved from a parent crystal of triglycine sulfate were etched in water until they were about 10^{-2} cm thick. Units about 3 mm square were cut from these etched slices and provided with circular evaporated gold electrodes, about 2 mm in diameter. For some of the studies, units were provided with a guard-ring electrode so as to avoid possible spurious results arising from the effects of fringing fields; these have been shown to be appreciable under certain conditions.[5]

The crystals were mounted in an oven, the temperature of which was indicated by a thermocouple that fed into the Y axis of an X-Y chart recorder. The chopped light beam used for generating the pyroelectric signal reached the crystal through a small window in the oven wall and the pyroelectric signal, after amplification and rectification, was applied to the X axis of the recorder. As the light falling on the crystal made its temperature slightly higher than that of the oven (by about 5°C), the thermocouple readings were corrected so as to bring the Curie point to 49.8°C, where appropriate.[6]

[1] A. G. Chynoweth, J. Appl. Phys. **27**, 78 (1956).
[2] A. G. Chynoweth, Acta Cryst. **10**, 511 (1957).
[3] A. G. Chynoweth, Phys. Rev. **102**, 1021 (1956).
[4] A. F. Devonshire, Phil. Mag. **40**, 1040 (1949).
[5] R. C. Miller and A. Savage, J. Appl. Phys. **30**, 808 (1959).
[6] S. Triebwasser, IBM J. Research Develop. **2**, 212 (1958).

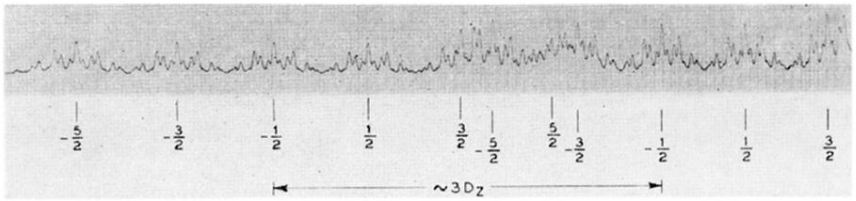

FIG. 3. A portion of the EPR spectrum of Mn^{++}:ZnF_2 observed at 23 kMc with $H_0 \| [001]$ and $T = 77°K$. (H_0 increases as one goes from left to right.) The magnetic quantum numbers belonging to the Mn^{55} hfs components of the electronic transition $M_s = -\frac{5}{2} \leftrightarrow M_s - 1 = -\frac{3}{2}$ are indicated in the upper row. Similarly the lower row of numbers identifies corresponding components in the $M_s = -\frac{3}{2} \leftrightarrow M_s - 1 = -\frac{1}{2}$ transition. The magnitude of the electronic fine structure splitting is $3D_z$. The separation of Mn^{55} hfs components is of order A^{55} and the super hfs due to the F^{19} nuclei is clearly visible on each Mn^{55} hfs component since $A^{19} < A^{55}$.

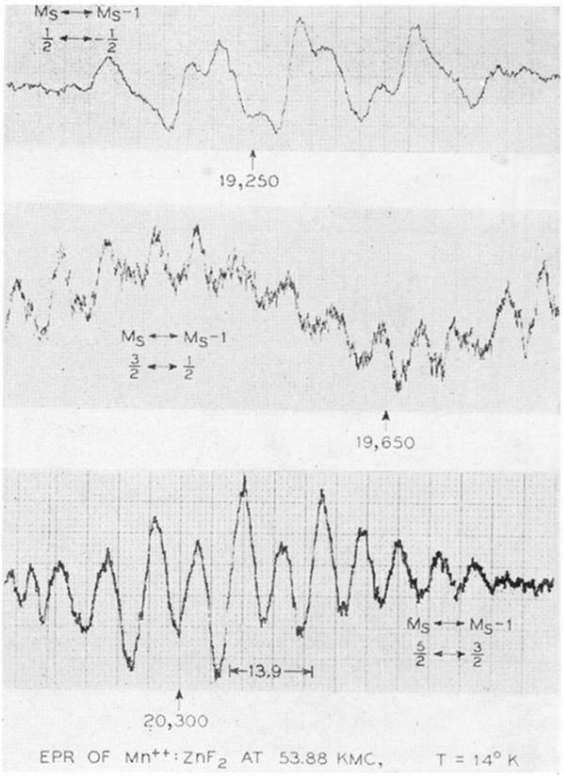

FIG. 6. Portions of the EPR spectrum of Mn^{++}:ZnF_2 at 54 kMc with $H_0 \| [001]$ and $T = 14°K$. The derivative of each of three hfs components is given for three distinct electronic transitions. The complexity in the spectra at 54 kMc is present in transitions which have the $M_s = +\frac{3}{2}$ level in common whereas for the same direction at 23 kMc the complexity was common to the transitions which had the $M_s = +\frac{1}{2}$ level in common. It is to be noticed that the two complex spectra are different at these frequencies both from each other and from the complex spectra observed at K band frequencies. The field separation indicated on the lowest transition in the figure corresponds to certain predicted values of the F^{19} hfs components for this electronic transition. Approximate values of H_0 are indicated on each recorded trace. Field inhomogeneities at these large applied fields unfortunately increase the line widths of each F^{19} hfs component.